

pubs.acs.org/crystal Article

Charge-Separated Metal—Organic Frameworks Derived from Boron-Centered Tetrapods

Sheela Thapa, Diane A. Dickie, and Yang Qin*



Cite This: Cryst. Growth Des. 2020, 20, 1598-1608



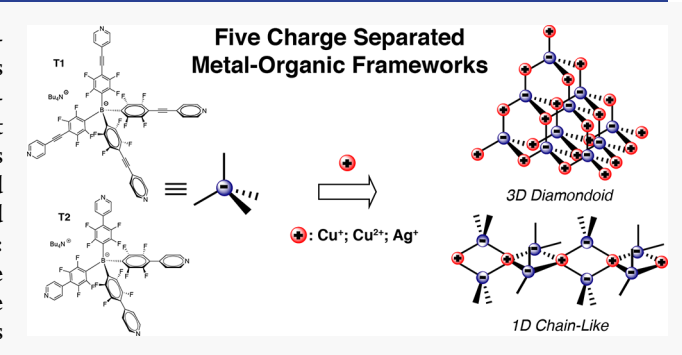
ACCESS

Metrics & More

Article Recommendations

Supporting Information

ABSTRACT: Metal—organic frameworks (MOFs) are an emerging class of microporous materials that have potential applications in a wide range of areas. As a subclass of MOFs, ionic MOFs, especially charge-separated MOFs, have been relatively less studied but possess unique features including strong host—guest interactions from the exposed charged centers. We report the synthesis and single-crystal structural characterization of five new charge-separated MOFs (UNM 1–5) based on two tetrapodal borate ligands: tetrakis(4-(4-pyridineethynyl)-2,3,5,6-tetrafluorophenyl)borate (T1) and tetrakis(4-(4-pyridyl)-2,3,5,6-tetrafluorophenyl)borate (T2) having rigid arms of different lengths and pyridine groups at the end of each arm. Coordination of these tetrapods with



Cu(I), Cu(II), and Ag(I) ions under specific conditions led to a series of new charge-separated MOFs in single crystalline forms. UNM-1 and UNM-2/UNM-3, which crystallize respectively in tetragonal $I\overline{4}$ space group and monoclinic C2/c space group, are derived from Cu(CH₃CN)₄BF₄ and Cu(NO₃)₂ upon coordination with T1. On the other hand, coordination of T2 with Cu(CH₃CN)₄BF₄ and AgBF₄ respectively yielded UNM-4 and UNM-5 in the monoclinic I2/a space group. All these MOFs possess several degrees of interpenetration that are correlated with the arm lengths of ligands. Noticeably, UNM-1 is 4-fold interpenetrated, leading to the highest stability among all five MOFs, while still displaying an impressive Brunauer–Emmett–Teller (BET) surface area (SA_{BET}) of ca. 621 m²/g. Our findings highlight the versatility of tetrapodal borate ligands in engineering charge-separated MOFs with diverse structures and controlled functionality.

■ INTRODUCTION

Crystal engineering is known as a scientific branch of exploring and understanding intermolecular interactions in the solid state and a powerful tool to design and construct ordered crystals with tailored properties. Since the late 20th century, crystal engineering has expanded into organic/inorganic hybrid materials and has led to the discovery of a new class of crystalline compounds known as metal-organic frameworks (MOFs) or porous coordination polymers (PCPs).²⁻⁶ MOFs are formed by coordination of rigid organic ligands to metal ions or clusters, leading to precisely controlled microporous crystals possessing large surface areas, tunable pore sizes and pore volumes, and versatile pore surface chemistry through articulate ligand designs. These unique properties make MOFs ideal candidates in a variety of applications including gas separation and storage, ^{10–13} catalysis, ^{14–16} chemical sensors, ^{17,18} medicines, ^{19–21} and electronics, ^{22–24} among many others. The majority of MOF research has been concentrated on the design and combination of different organic ligands and metals for the construction of new MOF materials with tailored structures and properties. By the judicious selection of metal nodes and ligand functionalities, a vast number of promising MOF materials with different dimensionalities and topologies have been created in the past.^{25–30} Most existing MOFs

are considered charge neutral in that the positive charges of metal ions are immediately balanced by surrounding anionic ligands, leading to the lack of accessible isolated ionic species within the pore volume or on the pore surfaces.

As a subclass of MOF materials, ionic MOFs contain exposed charged species within the pore environment, which can potentially lead to enhanced host—guest interactions caused by electric-field induced polarization of guest molecules and electrostatic and coordination interactions.^{31–34} The majority of existing ionic MOFs, containing a single type of charge covalently attached onto the pore surfaces, are built from charged organic ligands, either cationic or anionic, in addition to the neutral metal—ligand clusters, or secondary building units (SBUs). In order to ensure overall charge neutrality within these ionic MOFs, free charge-balancing counterions are commonly present within the pores, which will unavoidably reduce the pore sizes and make

Received: October 9, 2019 Revised: January 22, 2020 Published: January 23, 2020



Scheme 1. Chemical Structures of Borate Ligands T1 and T2

Scheme 2. Synthesis of T2

inclusion of guest molecules more difficult. One clever solution is to incorporate both positive and negative charges at precise locations with fixed separation distances within the MOF framework that is known as charge-separated or zwitterionic MOFs. The use of zwitterionic ligands containing both positive and negative species to bridge the metal ions is one of the most applied methods to prepare such MOFs. For example, existing charge-separated MOF materials have employed zwitterionic ligands containing both cationic (pyridinium, 35-45 imidazolium, 46,47 metalloporphyrin 48 or, ammonium 49) and common anionic moieties (e.g., carboxylate and sulfonate) to bind metals in different oxidation states, leading to charge-separated MOFs with or without the need for charge balancing free ions. Furthermore, anionic tetra(imidazolyl)borate ligands have been applied by Ziegler and co-workers for the synthesis of charge-separated MOFs for enclathration and anion exchange applications. 50-53 Borate ligands, being tetrahedral in geometry, are expected to result in three-dimensional materials upon metal binding, and the negative charge of borate anion can fully or partially compensate for the positive charges of metal ions, depending on their oxidation states.⁵⁴ In these structures, the offset angles between B-N and N-metal bonds of ca. 145°, as well as the rotational freedom of single bonds, can make construction of three-dimensional (3-D) structures difficult and hard to predict.⁵⁵ We have recently reported the synthesis of a tetrapodal borate ligand (T1, Scheme 1) having linear arms that successfully led to a charge-separated MOF (UNM-1) upon coordination with Cu⁺ ions. ⁵⁶ UNM-1 possesses 4-fold interpenetration, likely a result originating from the relatively large

arm lengths, which we believe can be alleviated by shortening the arms of the borate ligand.

In this paper we report the synthesis of a new borate ligand with shorter arms (T2, Scheme 1) and systematic studies of their coordination behaviors with different metals at different oxidation states. In addition to UNM-1, four single crystalline charge-separated MOFs are obtained by combining T1 or T2 with Cu(I), Cu(II), or Ag(I) metal cations. T2 indeed led to MOFs with fewer degrees of interpenetration but not necessarily with increased surface areas or stability. The uniqueness of our approach is the anionic borate ligand with straight arms for metal coordination, which can lead to predictable MOF structures in three dimensions, and the negative charges on borate centers that can counter balance the positively charged metal ions as well as form charge separation with fixed but tunable distances, i.e., the arm lengths of the borate ligands. These findings give us useful insights into the important relationships between ligand design and choices of metals and crystal structures and functions of charge-separated MOFs.

■ RESULTS AND DISCUSSION

Synthesis and Characterization of T1 and T2. T1 and compound 1 (Scheme 2) were synthesized according to previously reported procedures, ^{56–58} and the synthesis of T2 was accomplished in three steps as shown in Scheme 2, the details of which are provided in the Supporting Information. T2 is fully characterized by ¹H, ¹³C, ¹¹B, and ¹⁹F NMR spectroscopy (Supporting Information). Briefly, the presence of one tetrabutylammonium cation per borate center, i.e., per four

Table 1. Summary of Crystallographic Data and Selected Properties for UNM-1, UNM-2, and UNM-3

parameters	UNM-1	UNM-2	UNM-3
solvent of crystallization	CH ₂ Cl ₂ /CH ₃ CN	CH ₂ Cl ₂ /CH ₃ OH	H_2O/DMF
crystal yield (%)	74.4	74	27
complex with	$Cu(CH_3CN)_4BF_4$	$Cu(NO_3)_2 \cdot XH_2O$	$Cu(NO_3)_2 \cdot XH_2O$
color	yellow	blue	blue
shape	needle	rod	rod
chemical formula	$\mathrm{C_{52}H_{16}BCuF_{16}N_4}$	$C_{52}H_{18}BCuF_{16}N_4O$	$C_{110}H_{54}B_2CuF_{32}N_{10}O_6$
formula weight, g/mol	1075.04	1093.05	2304.79
temperature (K)	100(2)	100(2)	100(2)
crystal system	tetragonal	monoclinic	monoclinic
space group	$I\overline{4}$	C2/c	C2/c
a (Å)	a = 23.5586(7)	a = 29.313(3)	a = 36.891(3)
b (Å)	b = 23.5586(7)	b = 20.394(2)	b = 21.6194(16)
c (Å)	c = 24.6516(9)	c = 38.674(4)	c = 16.2556(13)
α (deg)	90	90	90
β (deg)	90	90.874(5)	103.126(5)
γ (deg)	90	90	90
$V(Å^3)$	13681.8(10)	23117.(4)	12626.1(17)
Z	8	8	4
$D_{\rm calc}$ (g/cm ³)	1.044	0.628	1.212
total reflections	31438	51445	47295
unique	12964 [R(int) = 0.0408]	9047 $[R(int) = 0.1971]$	9091 $[R(int) = 0.0846]$
function minimized	$\Sigma w (F_0^2 - F_c^2)^2$	$\Sigma w (F_{\rm o}^2 - F_{\rm c}^2)^2$	$\Sigma w(F_{\rm o}^2 - F_{\rm c}^2)^2$
data/restraints/parameters	12964/0/668	9047/603/679	9091/0/732
goodness-of-fit on F^2	0.937	1.214	1.007
$R_1 \ (I > 2\sigma(I), \ wR_2$	0.0314, 0.0657	0.1014, 0.2471	0.0603, 0.1552
R_1 , wR_2 (all data)	0.0459, 0.0697	0.2338, 0.3117	0.1183, 0.1862
surface area (m ² /g)	621	40	N/A

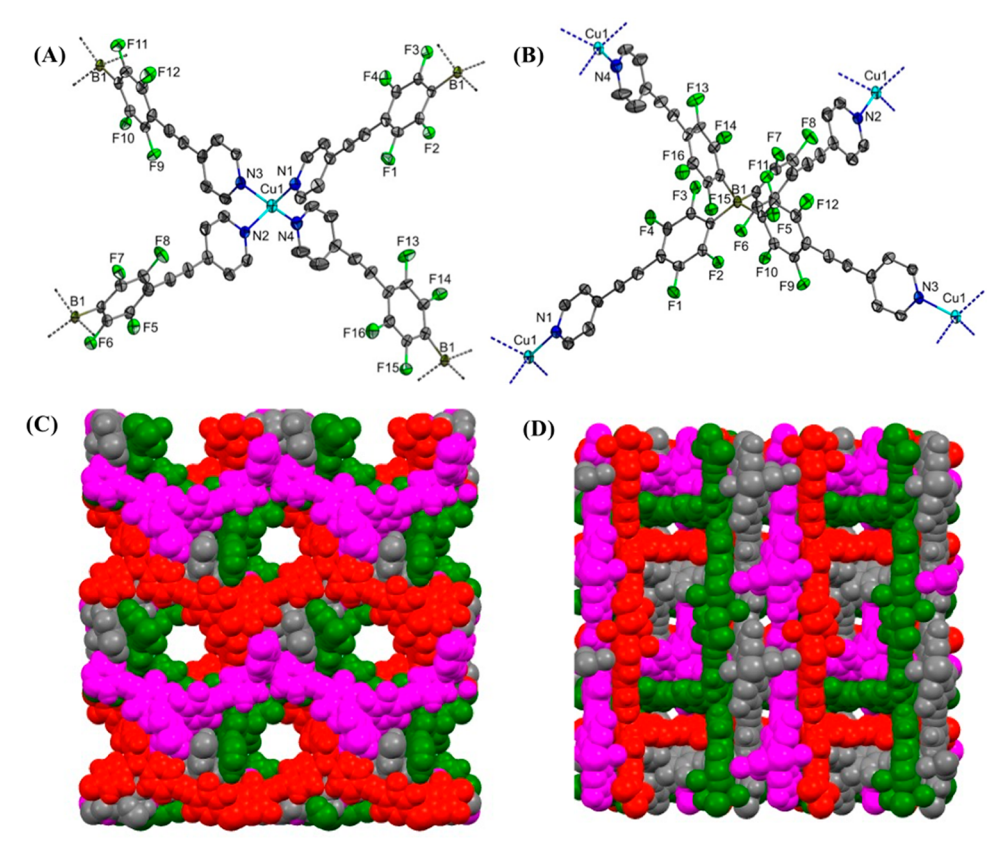


Figure 1. Single crystal X-ray structure of UNM-1: (A) partial view of crystal structure showing coordination environment around copper; (B) partial view of crystal structure showing coordination environment around boron; (C) space-filling model of a $2 \times 2 \times 2$ unit cell viewed from the Y-axis; and (D) space-filling model of a $2 \times 2 \times 2$ unit cell viewed from the Z-axis, all showing 4-fold interpenetration as revealed by the red, green, gray, and magenta color coding. Carbon atoms appear in gray, nitrogen in blue, boron in yellow, fluorine in green, and copper in cyan. Hydrogen atoms are omitted for clarity.

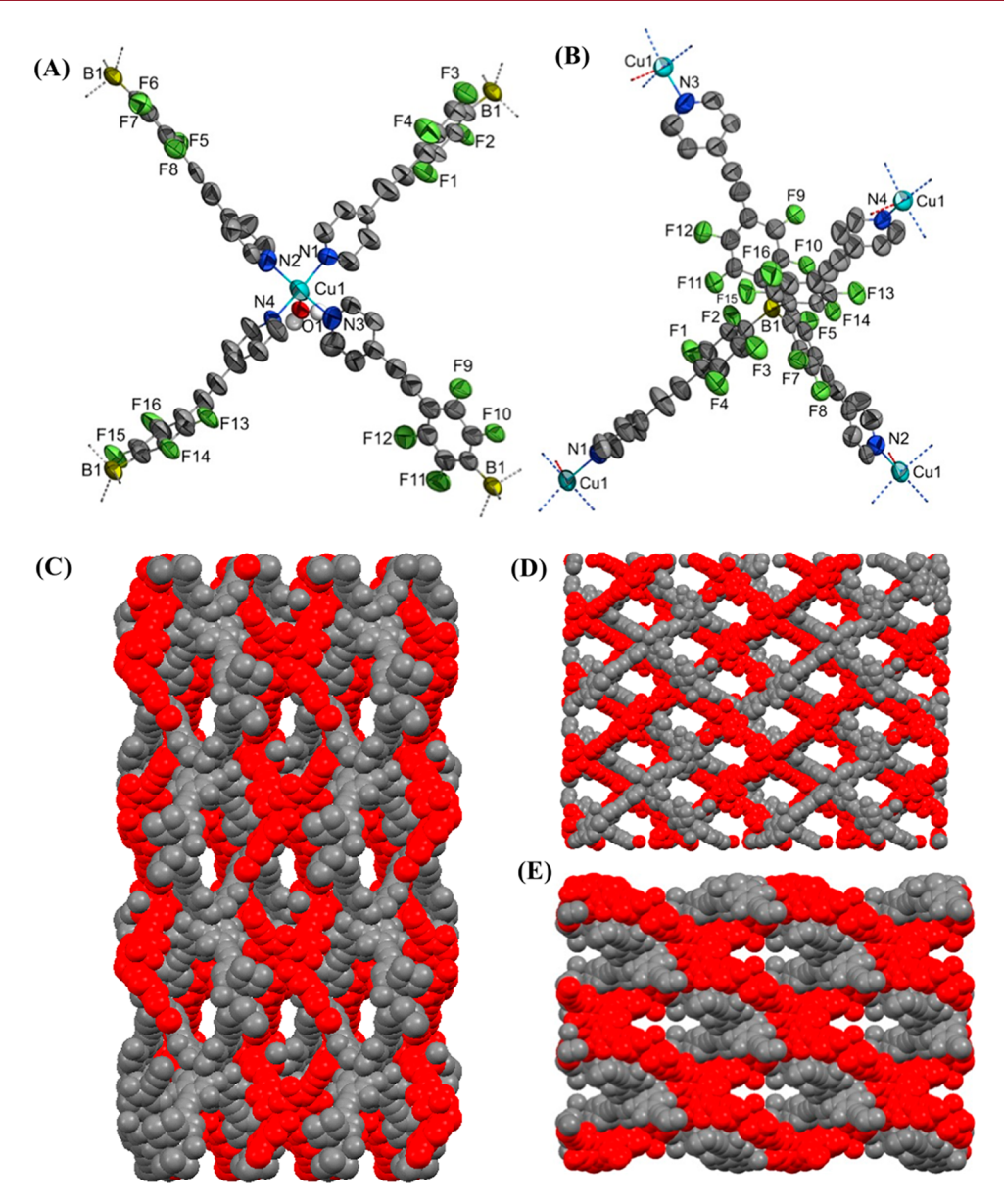


Figure 2. Single crystal X-ray structure of UNM-2. (A) Partial view of the crystal structure showing coordination environment around copper; (B) coordination environment around boron; (C) space-filling model of a $2 \times 2 \times 2$ unit cell viewed from the X-axis; (D) space-filling model of a $2 \times 2 \times 2$ unit cell viewed from the Y-axis, and (E) space-filling model of a $2 \times 2 \times 2$ unit cell viewed from the Z-axis, all showing 2-fold interpenetration as revealed by the red and gray color coding. Atoms of carbon appears in gray, nitrogen in blue, boron in yellow, fluorine in green, oxygen in red, and copper in cyan. Hydrogen atoms are omitted for clarity.

pyridine groups, is confirmed by proton NMR integration. ¹¹B NMR shows a sharp signal at -16.3 ppm, consistent with the tetra-coordinated environment on the boron atom. 19F NMR displays two sharp signals at -129.9 and -146.8 ppm, consistent with those from ligand T1. In the ¹³C NMR spectrum, the F₄-phenyl carbon atoms ortho- and meta- to the boron center appears as two sets of doublets at 147.8 and 142.4 ppm having ${}^{1}J_{CF}$ coupling constants of 252 and 251 Hz, respectively. The broad signal ranging from 132 to 134 ppm is assigned to the ipso-carbon atom that is split by ¹J boron and ²J fluorine coupling, respectively. The triplet at 113.1 ppm is then assigned to the F_4 -phenyl carbon para to the boron center with a ${}^2J_{CF}$ coupling constant of 15 Hz. The sharp signals with large intensities at 149.9, 137.4, and 124.9 ppm are from the pyridine rings, while all other carbons from tetrabylammonium group are observed in between 13 and 59 ppm.

We then attempted crystallization experiments by using T1 and T2 as ligands in combination with Cu(I), Cu(II), and Ag(I) ions under various conditions. While not all combinations led to X-ray quality single crystals, we were able to obtain five different crystals with distinct structures and physical characteristics. We discuss and compare the synthesis and structures of each of these MOF crystals in the following sections

Synthesis and Structural Analyses of UNM-1. Yellow, needle-shaped single crystals of UNM-1 were obtained by slow diffusion of an acetonitrile solution of $Cu(CH_3CN)_4BF_4$ into a dichloromethane solution of T1 over a period of 48 h at room temperature. Since the coordination environment around both boron and Cu(I) atoms is tetrahedral, we expected the formation of a diamondoid like 3-D network containing alternating positively charged Cu(I) and negatively charged boron nodes,

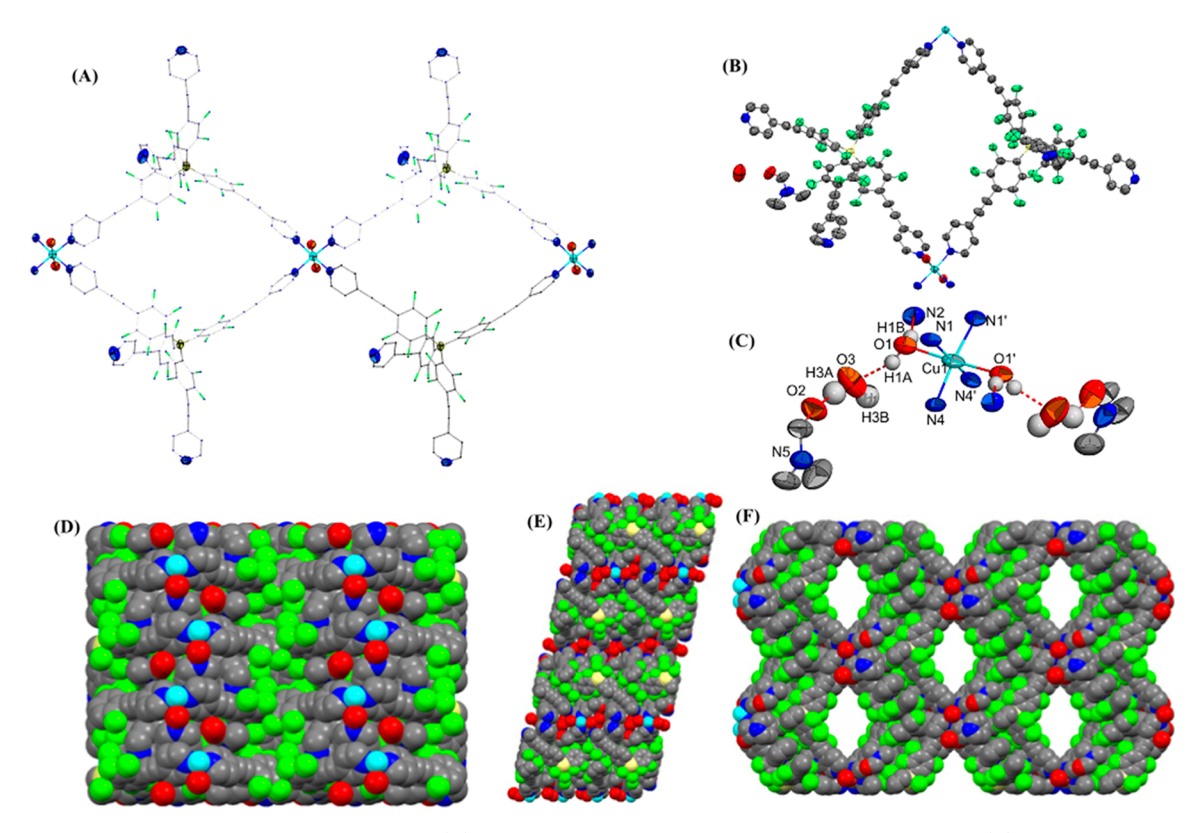


Figure 3. Single crystal X-ray structure of UNM-3; (A) framework structure showing a chainlike structure; (B) a crystalline unit showing coordination environment around the boron (C) coordination environment around copper and hydrogen bonding between solvent molecules; (D) space-filling model of a $2 \times 2 \times 2$ unit cell viewed from the X-axis; (E) space-filling model of a $2 \times 2 \times 2$ unit cell viewed from the X-axis, Atoms of carbon appear in gray, nitrogen in blue, boron in yellow, fluorine in green, oxygen in red, and copper in cyan. Hydrogen atoms are omitted for clarity.

leading to a charge-separated MOF without free ions. This hypothesis is confirmed by detailed single crystal X-ray analysis, and the results are summarized in Table 1, Figure 1, and Figure S9. The composition of the crystal was found to be C₅₂H₁₆BCuF₁₆N₄, which is consistent with the proposed coordination structure. The crystal system of UNM-1 is tetragonal with space group I4. The dihedral angles around boron centers range from ca. 101° to 116° and those around copper centers from ca. 100° to 121° indicating that the coordination environment around both Cu(I) and boron atoms is approximately tetrahedral (Figure 1A,B). The average boron-copper distance is measured at ca. 13.3 Å, which is long enough to result in the 4-fold interpenetration as shown in Figure 1C,D. Channels with two different sizes are revealed from the space filling models. The larger pores with a diameter of ca. 7.4 Å are seen along the X or Y axis, while viewing along the Z axis shows pores with a diameter of ca. 2.7 Å. UNM-1 is stable upon solvent removal as confirmed by powder XRD (PXRD) measurements as shown in Figure S15, in which the PXRD patterns of UNM-1 after treatment under high vacuum closely match those from simulation. About 100 mg of UNM-1 was outgassed at 60 °C under a vacuum with durations determined by the gas analyzer's protocol before conducting the Brunauer-Emmett-Teller (BET) gas adsorption analyses. Despite the 4-fold interpenetration, the surface area of UNM-1 is found to be ca. 621 m²/g, which is one of the highest among 4-fold interpenetrated networks^{59,60} and is likely a result of the absence of free ions.

Synthesis and Structural Analyses of UNM-2. Two different crystal systems, namely, UNM-2 and UNM-3, were obtained by combining T1 and $Cu(NO_3)_2$ depending on the

solvents used during synthesis. Slow diffusion of a methanol solution of Cu(NO₃)₂ into a dichloromethane solution of T1 during the course of 48 h at room temperature resulted in the formation of blue rod shaped crystals, i.e., UNM-2. Crystallographic data and crystal structures of UNM-2 are presented in Table 1, Figure 2, and Figure S10. UNM-2 has an approximate composition of C₅₂H₁₈BCuF₁₆N₄O and crystallizes in a monoclinic crystal system with a space group of C2/c. As shown in Figure 2, the copper atoms in UNM-2 are coordinated to 4 pyridyl units from different borate ligands and one water molecule, resulting in a square pyramidal geometry. Since the copper atoms in UNM-2 are in +2 oxidation state and the equally numbered borate units possess a -1 charge, there must be one -1 charged counterion, likely NO₃⁻ ions, per Cu(II) atom within the framework in order to ensure the overall charge neutrality. Because these nitrate ions are disordered and potentially mobile, they could not be resolved in the single crystal X-ray analyses. To further confirm the existence of the NO₃⁻ counterions, we first performed elemental analysis on UNM-2 (Supporting Information). Despite relatively large errors in H content, the found C (53.57%) and N (5.75%) contents respectively match better with those calculated for $C_{52}H_{18}BCuF_{16}N_5O_4$ (C 54.07%, N 6.06%), i.e., including one NO₃ ion per Cu atom, than those calculated for C₅₂H₁₈BCuF₁₆N₄O (C 57.14%, N 5.13%) without including the $\mathrm{NO_3}^-$ ion. We have also performed IR spectroscopy measurements on UNM-2 powders in KBr pellets, and the result is shown in Figure S14 (Supporting Information). A sharp peak with intermediate intensity at ca. 1384 cm⁻¹ is observed, which corresponds to the N-O stretching mode of the NO₃⁻ ion.

The N-Cu-N bond angles average at ca. 116°, and the N-Cu-O bond angles are at ca. 96°. The bond angles around boron atoms range from 100° to 116°, similar to those found in UNM-1. The Cu-OH₂ bond length in UNM-2 is found at ca. 2.52 Å, and the Cu-N distances range from 2.02 to 2.09 Å. The boron-boron and boron-copper distances are measured at about 21.2 and 13.25 Å, respectively. Despite the same ligand arm lengths as in UNM-1, UNM-2 is found to be 2-fold interpenetrated as shown in Figure 2C-E. The reduced degree of interpenetration is likely caused by the inclusion of the nitrate ions in the framework, which also possibly led to a relatively small BET surface area of ca. 40.3 m²/g despite the pore sizes of 10.7 Å (viewed from X-axis), 10.27 Å (viewed from Y-axis) and 14.06 Å (viewed from Z-axis) (Figure 2C-E). To be noticed, about 100 mg of UNM-2 was outgassed at 60 °C under a vacuum with durations determined by the gas analyzer's protocol before conducting the BET gas adsorption analyses. In addition, UNM-2 is not stable upon solvent removal under a high vacuum as confirmed by PXRD measurements as shown in Figure S16.

Synthesis and Structural Analyses of UNM-3. When a DMF solution of T1 and a water solution of $Cu(NO_3)_2$ were slowly mixed and was left to stand undisturbed for 15 days at room temperature, light blue rod shaped crystals of UNM-3 were obtained. Crystallographic data and crystal structures are presented in Table 1, Figure 3, and Figure S11. The approximate crystal composition of UNM-3 is C₁₁₀H₅₄B₂CuF₃₂N₁₀O₆, indicating the presence of water and DMF molecules within the crystal structures. The crystal system of UNM-3 is monoclinic with a space group of C2/c. The Cu²⁺ center is coordinated to four pyridyl groups from different ligands and to two water molecules in trans positions, resulting in an octahedral geometry as shown in Figure 3. The C-B-C angle around the boron atom ranges from ca. 100° to 114°, consistent with the tetrahedral coordination environment of boron atoms. The cis N-Cu-N angle and N-Cu-O angle around the copper center ranges from ca. $87-92^{\circ}$ and ca. $88-94^{\circ}$ respectively. All the Cu-N bond lengths are normal as found in other copper pyridyl complexes (2.017 and 2.027 Å).61-63 However, the diaxial Cu-OH₂ bond length in UNM-2 is ca. 2.45 Å and lengthened, demonstrating possible Jahn-Teller distortion because of the d⁹ configuration of Cu(II) in UNM-3. The length of diaxial Cu-O bond in UNM-3 is compared with the Cu-O bond length (2.014-2.084 Å) in hexaaquacopper(II) complexes without the Jahn-Teller effect. 64,65 Although the ligand T1 is tetrahedral in shape and expected to form 3D MOF structures upon coordination with metal centers, UNM-3 is found to be a one-dimensional coordination polymer. In UNM-3, only two out of the four pyridine arms of each T1 ligand are coordinated to the copper atoms, leaving the other two dangling, which leads to a chain-like structure. Because of the extensive H-bonding interactions between the ligand N atoms and coordinated solvent molecules, the crystal structure of UNM-3 is not continuous in all three dimensions, but instead forms one-dimensional chain-like structures. As shown in Figure 3C, two of the four pyridine N atoms (N1 and N4) coordinating to copper sit on a 2-fold rotation axis. A third pyridine N (N2) is hydrogen bonded to the water molecule (O1) that is also coordinated to copper. This O1 water molecule also hydrogen bonds to an uncoordinated water (O3), and the uncoordinated water makes a hydrogen bond to a DMF molecule (O2). The fourth and final pyridine N3 and the hydrogen atoms on the nearby O3 water molecule do not

Table 2. Summary of Crystallographic Data and Selected Properties of UNM-4 and UNM-5

parameters	UNM-4	UNM-5
solvent of crystallization	CH ₂ Cl ₂ /CH ₃ CN	CH ₂ Cl ₂ /CH ₃ CN
crystal yield (%)	84	77
complex with	Cu(CH ₃ CN) ₄ BF ₄	Ag BF ₄
color	yellow	colorless
shape	needle	needle
chemical formula	$C_{44}H_{16}BCuF_{16}N_4$	$C_{44}H_{16}AgBF_{16}N_4$
formula weight, g/mol	978.96	1023.29
temperature (K)	100(2)	100(2)
crystal system	monoclinic	monoclinic
space group	I2/a	I2/a
a (Å)	a = 15.6357(11) Å	a = 15.197(3) Å
b (Å)	b = 29.2695(12) Å	b = 30.954(4) Å
c (Å)	c = 16.0766(7) Å	c = 16.340(2) Å
α (deg)	90	90
β (deg)	98.025(2)	100.440(2)
γ (deg)	90	90
V (Å ³)	7285.4(7)	7559.(2)
Z	4	4
$D_{\rm calc}~({ m g/cm^3})$	0.893	0.899
total reflections	28037	54294
unique	6707 [R(int) = 0.1530]	7227 [R(int) = 0.1635]
function minimized	$\Sigma w (F_{\rm o}^2 - F_{\rm c}^2)^2$	$\Sigma w (F_{\rm o}^2 - F_{\rm c}^2)^2$
data/restraints/ parameters	6707/276/299	7227/0/299
goodness-of-fit on F ²	0.914	1.003
R_1 $(I > 2\sigma(I), wR_2$	0.0726, 0.1892	0.0646, 0.1698
R_1 , wR_2 (all data)	0.1725, 0.2319	0.1865, 0.2323
surface area $\left(m^2/g\right)$	9	3

appear to form hydrogen bonds nor coordinate to anything. Attempts to determine the porosity of UNM-3 failed to generate any meaningful results since solvent removal under high vacuum resulted in amorphous materials by PXRD analysis (Figure S17). From a single crystal structure, the framework appears nonporous along the X and Y-axis while along the Z-axis the pore size is ca. 9.26 Å.

Synthesis and Structural Analyses of UNM-4. Slow mixing of a T2 solution in dichloromethane and a Cu-(CH₃CN)₄BF₄ solution in acetonitrile followed by standing still for 48 h at room temperature afforded needle-shaped yellow crystals of UNM-4 that were big enough to be characterized by single crystal X-ray diffraction. The three-dimensional framework formed by bridging of copper(I) to anionic borate formed a charge neutral framework with an approximate composition of C₄₄H₁₆BCuF₁₆N₄. Crystallographic data and crystal structures are presented in Table 2, Figure 4, and Figure S12. UNM-4 is in a monoclinic crystal system with a space group of I2/a. The use of T2 without the triple bonds led to UNM-4 with 2-fold interpenetration, which is half that of UNM-1 and supports our hypothesis that shorter ligands can lead to fewer degrees of interpenetration. The separation distance between the boron centers of two ligands sharing a common copper atom is ca. 17.64(7) Å, and the boron-copper distance is ca. 10.8 Å, which is large enough to accommodate such 2-fold interpenetration. A space filling model of 2 × 2 × 2 unit cell displaying interpenetration is shown in Figure 4C-E. In UNM-4, both boron and copper have a tetrahedral coordination environment. Each copper atom is coordinated to four pyridyl units from different borate ligands and vice versa, and the Cu-N distances are between 2.01 and 2.03 Å. The

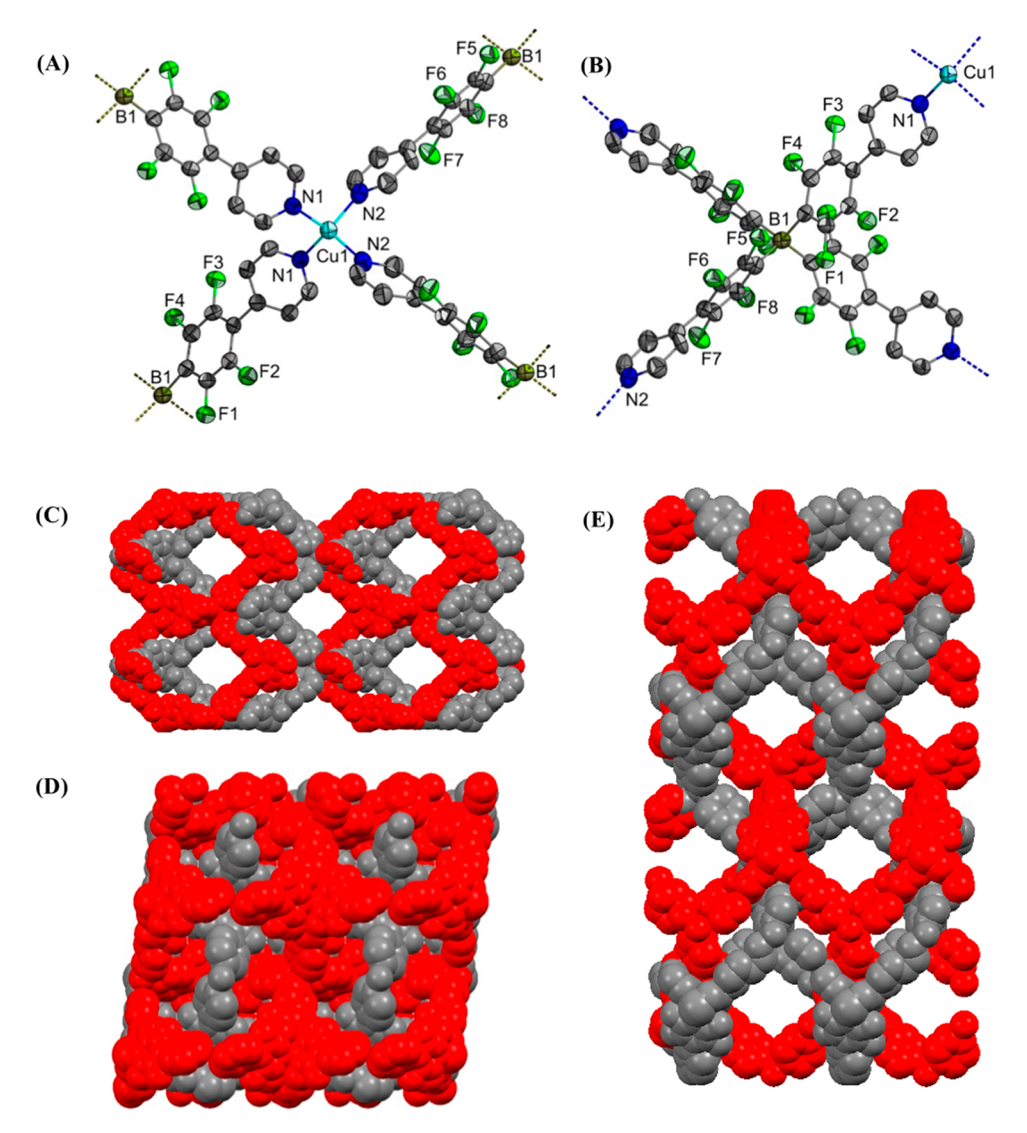


Figure 4. Single crystal X-ray structure of UNM-4; (A) partial view of crystal structure showing coordination environment around copper; (B) coordination environment around boron; (C) space-filling model of a $2 \times 2 \times 2$ unit cell viewed from the X-axis; (D) space-filling model of a $2 \times 2 \times 2$ unit cell viewed from the Z-axis, all showing 2-fold interpenetration as revealed by the red and gray color coding. Atoms of carbon appear in gray, boron in yellow, fluorine in green, and copper in cyan. Hydrogen atoms are omitted for clarity.

bond angles around boron centers range from ca. 102° to 116°, and those around copper centers are from ca. 101° to 119°. Compared to UNM-1, UNM-4 has very low porosity. About 100 mg of UNM-4 was outgassed at 60 °C under a vacuum with durations determined by the gas analyzer's protocol before conducting the BET gas adsorption analyses. The BET surface area of UNM-4 is ca. $9 \text{ m}^2/\text{g}$. On the basis of the single crystal structure, the framework is nonporous when viewed from the Y-axis, but when viewed from the X- and Z-axis, the pore sizes were found as ca. 13.05 Å and ca. 11.09 Å respectively. The relatively small BET surface area value is likely caused by structural collapse during the solvent removal process. We have thus attempted to dry UNM-4 at −78 °C undera high vacuum for 48 h, and the PXRD pattern is shown in Figure S18. The signals from low temperature drying samples match the simulated pattern and appear slightly more resolved than those dried at room temperature. However, BET measurements still show negligible differences between samples dried at different temperatures. This suggests that

the structure of UNM-4 is not stable upon solvent removal even at low temperature and slow evaporation rates.

Synthesis and Structural Analyses of UNM-5. In order to see if replacing a copper ion from the framework with a bigger metal ion can bring any changes in the crystal structure, a new MOF named UNM-5 was synthesized from T2 and AgBF₄. UNM-5 is a colorless, rod-shaped crystal formed by the slow diffusion of T2 solution in dichloromethane and $AgBF_{4}$ solution in acetonitrile for 48 h at room temperature. The approximate composition of UNM-5 is C₄₄H₁₆BAgF₁₆N₄, and it crystallizes in the monoclinic crystal system with a space group of I2/a. Crystal structures and crystallographic data are presented in Figure 5, Table 2, and Figure S13. Similar to UNM-1 and UNM-4, it is formed as a charge neutral framework as the +1 charge of silver cation is compensated by the -1 charge of boron anion. In UNM-5, silver is coordinated tetrahedrally to four pyridyl groups from different borate ligands, and the bond angles around the silver atom range from ca. 95° to 128° . The coordination environment around boron

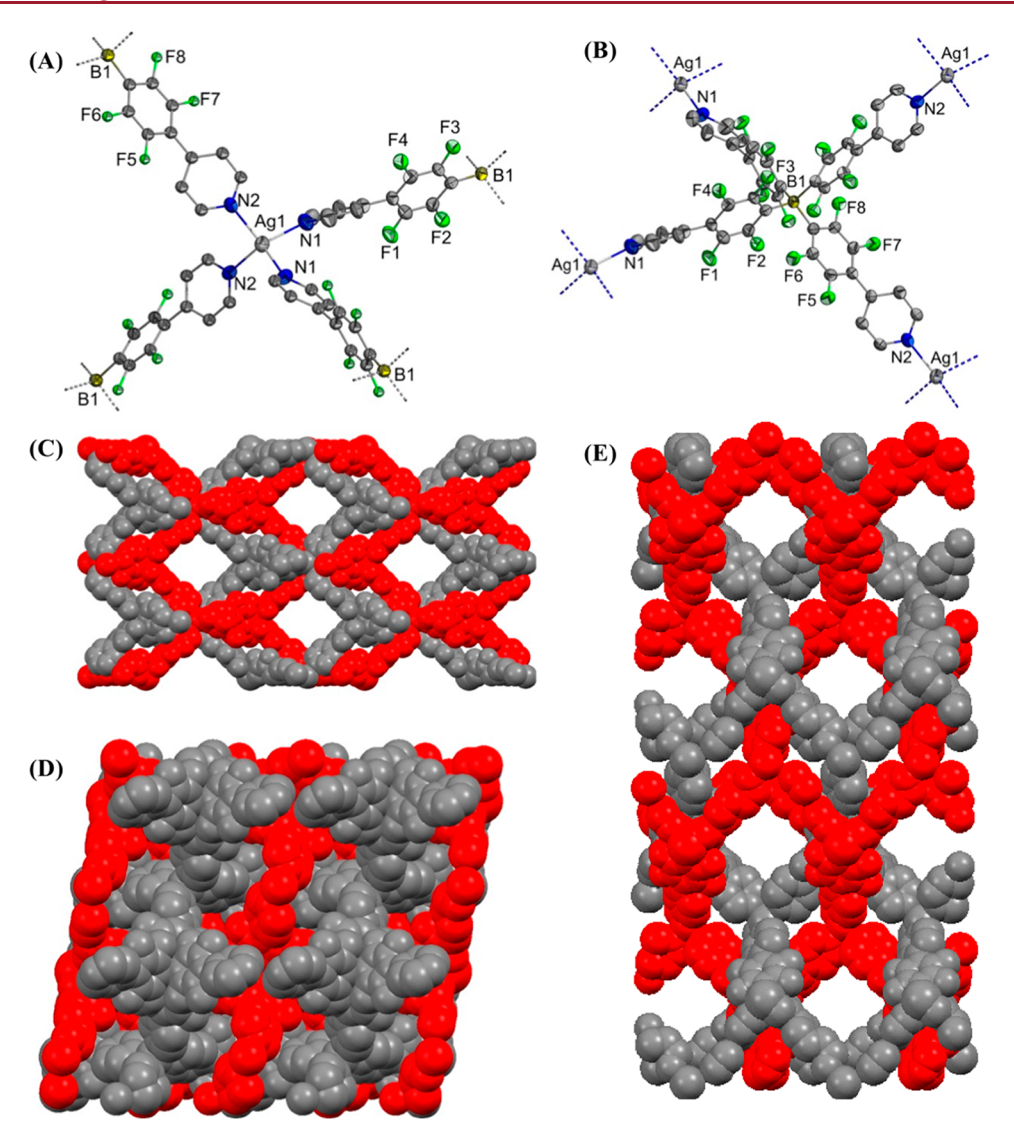


Figure 5. Single crystal X-ray structure of UNM-5; (A) partial view of crystal structure showing the coordination environment around copper; (B) coordination environment around boron; (C) space-filling model of a $2 \times 2 \times 2$ unit cell viewed from the X-axis; (D) space-filling model of a $2 \times 2 \times 2$ unit cell viewed from the Y-axis; and (E) space-filling model of a $2 \times 2 \times 2$ unit cell viewed from the Z-axis, all showing 2-fold interpenetration as revealed by the red and gray color coding. Atoms of carbon appear in gray, boron in yellow, fluorine in green, and silver in light gray. Hydrogen atoms are omitted for clarity.

is also tetrahedral with C-B-C angles of ca. 101° to 115°. The separation distance between the boron-boron of two ligands bonded to same silver atom is ca. 18.2 Å and boronsilver is ca. 11.09 Å, which are bigger than those of UNM-4 and are consistent with the use of larger silver atoms. UNM-5 is 2-fold interpenetrated as shown in Figure 5C-E. About 100 mg of UNM-5 was outgassed at 60 °C under a vacuum with durations determined by the gas analyzer's protocol before conducting the BET gas adsorption analyses. The BET surface area of UNM-4 is very low as ca. 3 m²/g, indicating that the crystals are less porous after solvent removal. The single crystal structure of the framework appears nonporous from Y-axis, but from X- and Z-axis, the pore sizes were found as ca. 13.73 Å and ca. 10.56 Å respectively. The relatively small BET surface area value is likely caused by structural collapse during the solvent removal process. We have thus attempted to dry UNM-5 at -78 °C under a high vacuum for 48 h, and the PXRD pattern is shown in Figure S19. The signals from low temperature drying samples match the simulated pattern and

appear slightly more resolved than those dried at room temperature. However, BET measurements still show negligible differences between samples dried at different temperatures. This suggests that the structure of UNM-5 is not stable upon solvent removal even at low temperature and slow evaporation rates.

CONCLUSIONS

In conclusion, borate-centered tetrapodal ligands are effective for the construction of a series of charge-separated MOFs. By employing a solvent diffusion crystallization technique, five different MOFs, namely, UNM-1, UNM-2, UNM-3, UNM-4, and UNM-5, are synthesized from two borate ligands possessing different arm lengths. All these MOFs crystallized in different space groups depending upon the oxidation states of metal ions. Among all MOFs, UNM-1 formed from Cu(I) and T1 is the most stable and possesses the largest surface area of $621 \text{ m}^2/\text{g}$, despite the 4-fold interpenetrated structure. Replacing Cu(I) with Cu(II) led to the formation of UNM-2 that is a 2-fold interpenetrated framework with a small surface

area of 40.3 m²/g, likely caused by the presence of chargebalancing nitrate anions inside the pores. Although both UNM-2 and UNM-3 were synthesized from the same metal and ligand precursors and crystallized in the same space group, the use of DMF in the crystallization process seems to lead to large structural changes. Unlike UNM-2, UNM-3 contains onedimensional coordination chains loosely held together by hydrogen bonding interactions between pyridine ligand, water, and DMF molecules. As a result, UNM-3 is very unstable after solvent removal due to the loss of coordinated solvents under a vacuum. In order to reduce the degrees of interpenetration, we removed the ethynyl bonds in T1 and synthesized a new tetrahedral ligand T2 with shorter arms. Indeed, when T2 is coordinated with Cu(I) and Ag(I), both the resulting UNM-4 and UNM-5 possess 2-fold interpenetration as compared with the 4-fold interpenetration in UNM-1. Both of these materials are crystallized in a monoclinic crystal system with a similar space group of I2/a. Although both UNM-4 and UNM-5 are charge neutral without the need for free charge-balancing ions, both frameworks have relatively low surface areas and are unstable after solvent removal, likely caused by the reduced degrees of interpenetration. Thus, we have estimated the amount of solvent molecules present in the channels of MOFs based on electron density and the solvents used during syntheses. There are up to 14 molecules of acetonitrile in the asymmetric unit of UNM-1, up to 38 molecules of methanol in UNM-2, and perhaps two molecules each of DMF and water in UNM-3. For UNM-4 and UNM-5, the situation is less clear because the solvents were mixtures of dichloromethane and acetonitrile, and it is not possible to tell how much each solvent was trapped in the pores. We just know that the solvent had up to 219 electrons in UNM-4 and 318 in UNM-5. Our results demonstrate the potential of tetrapodal anionic borate ligands in construction of charge-separated MOFs with unique architectures and properties. Shorter ligands expectedly lead to lower degrees of interpenetration but not necessarily higher stability or surface areas. The materials properties are closely related to the crystal structural details that are sensitive to the subtle changes in experimental condition including metal oxidation states, crystallization methodologies, and solvent additives.

ASSOCIATED CONTENT

Supporting Information

The Supporting Information is available free of charge at https://pubs.acs.org/doi/10.1021/acs.cgd.9b01340.

Synthetic details; NMR spectra; single crystal data; powder XRD data; IR spectrum (PDF)

Accession Codes

CCDC 1865216 (UNM-1), 1945949 (UNM-2), 1945951 (UNM-3), and 1945960—1945961 (UNM-4 and UNM-5) contain the supplementary crystallographic data for this paper. These data can be obtained free of charge via www.ccdc.cam.ac.uk/data_request/cif, or by emailing data_request@ccdc.cam.ac.uk, or by contacting The Cambridge Crystallographic Data Centre, 12 Union Road, Cambridge CB2 1EZ, UK; fax: +44 1223 336033.

AUTHOR INFORMATION

Corresponding Author

Yang Qin – Department of Chemistry & Chemical Biology, University of New Mexico, Albuquerque, New Mexico 87131, *United States;* orcid.org/0000-0002-5764-8137; Email: yangqin@unm.edu

Authors

Sheela Thapa — Department of Chemistry & Chemical Biology, University of New Mexico, Albuquerque, New Mexico 87131, United States

Diane A. Dickie — Department of Chemistry & Chemical Biology, University of New Mexico, Albuquerque, New Mexico 87131, United States; Oorcid.org/0000-0003-0939-3309

Complete contact information is available at: https://pubs.acs.org/10.1021/acs.cgd.9b01340

Notes

The authors declare no competing financial interest.

ACKNOWLEDGMENTS

The U.S. National Science Foundation (DMR-1453083 and CHE-1904659) is acknowledged for financial support for this research.

REFERENCES

- (1) Desiraju, G. R. Supramolecular Synthons in Crystal Engineering—A New Organic Synthesis. *Angew. Chem., Int. Ed. Engl.* **1995**, 34, 2311–2327.
- (2) Eddaoudi, M.; Moler, D. B.; Li, H.; Chen, B.; Reineke, T. M.; O'Keeffe, M.; Yaghi, O. M. Modular Chemistry: Secondary Building Units as a Basis for the Design of Highly Porous and Robust Metal—Organic Carboxylate Frameworks. *Acc. Chem. Res.* **2001**, *34*, 319–330.
- (3) Moulton, B.; Zaworotko, M. J. From Molecules to Crystal Engineering: Supramolecular Isomerism and Polymorphism in Network Solids. *Chem. Rev.* **2001**, *101*, 1629–1568.
- (4) Kitagawa, S.; Kitaura, R.; Noro, S.-I. Functional Porous Coordination Polymers. *Angew. Chem., Int. Ed.* **2004**, 43, 2334–2375.
- (5) Furukawa, H.; Cordova, K. E.; O'Keeffe, M.; Yaghi, O. M. The Chemistry and Applications of Metal-Organic Frameworks. *Science* **2013**, *341*, 1230444.
- (6) Kitagawa, S. Future Porous Materials. Acc. Chem. Res. 2017, 50, 514-516.
- (7) Batten, S. R.; Champness, N. R.; Chen, X.-M.; Garcia-Martinez, J.; Kitagawa, S.; Öhrström, L.; O'Keeffe, M.; Suh, M. P.; Reedijk, J. Terminology of Metal-Organic Frameworks and Coordination Polymers (IUPAC Recommendations. *Pure Appl. Chem.* **2013**, *85*, 1715–1724.
- (8) Kaskel, S. The Chemistry of Metal-Organic Frameworks. Synthesis, Characterization, and Applications; Wiley-VCH Verlag GmbH & Co.: Weinheim, Germany, 2016.
- (9) Yaghi, O. M.; Kalmutzki, M. J.; Diercks, C. S. Introduction to Reticular Chemistry: Metal-Organic Frameworks and Covalent Organic Frameworks; Wiley-VCH Verlag: Weiheim, Germany, 2019.
- (10) Shah, M.; McCarthy, M. C.; Sachdeva, S.; Lee, A. K.; Jeong, H.-K. Current Status of Metal-Organic Framework Membranes for Gas Separations: Promises and Challenges. *Ind. Eng. Chem. Res.* **2012**, *51*, 2179–2199
- (11) Trickett, C. A.; Helal, A.; Al-Maythalony, B. A.; Yamani, Z. H.; Cordova, K. E.; Yaghi, O. M. The Chemistry of Metal-Organic Frameworks for CO2 Capture, Regeneration and Conversion. *Nat. Rev. Mater.* **2017**, *2*, 17045.
- (12) Kumar, K. V.; Preuss, K.; Titirici, M.-M.; Rodriguez-Reinoso, F. Nanoporous Materials for the Onboard Storage of Natural Gas. *Chem. Rev.* **2017**, *117*, 1796–1825.
- (13) Kang, Z.; Fan, L.; Sun, D. Recent Advances and Challenges of Metal-Organic Framework Membranes for Gas Separation. *J. Mater. Chem. A* **2017**, *5*, 10073–10091.
- (14) Lee, J. Y.; Farha, O. K.; Roberts, J.; Scheidt, K. A.; Nguyen, S. T.; Hupp, J. T. Metal-Organic Framework Materials as Catalysts. *Chem. Soc. Rev.* **2009**, *38*, 1450–1459.

- (15) Zhu, L.; Liu, X.-Q.; Jiang, H.-L.; Sun, L.-B. Metal—Organic Frameworks for Heterogeneous Basic Catalysis. *Chem. Rev.* **2017**, *117*, 8129—8176.
- (16) Huang, Y.-B.; Liang, J.; Wang, X.-S.; Cao, R. Multifunctional Metal—Organic Framework Catalysts: Synergistic Catalysis and Tandem Reactions. *Chem. Soc. Rev.* **2017**, *46*, 126—157.
- (17) Kreno, L. E.; Leong, K.; Farha, O. K.; Allendorf, M.; Van Duyne, R. P.; Hupp, J. T. Metal-Organic Framework Materials as Chemical Sensors. *Chem. Rev.* **2012**, *112*, 1105–1125.
- (18) Wang, B.; Lv, X.-L.; Feng, D.; Xie, L.-H.; Zhang, J.; Li, M.; Xie, Y.; Li, J.-R.; Zhou, H.-C. Highly Stable Zr(IV)-Based Metal—Organic Frameworks for the Detection and Removal of Antibiotics and Organic Explosives in Water. *J. Am. Chem. Soc.* **2016**, *138*, 6204–6216.
- (19) Horcajada, P.; Gref, R.; Baati, T.; Allan, P. K.; Maurin, G.; Couvreur, P.; Ferey, G.; Morris, R. E.; Serre, C. Metal-Organic Frameworks in Biomedicine. *Chem. Rev.* **2012**, *112*, 1232–1268.
- (20) He, C.; Liu, D.; Lin, W. Nanomedicine Applications of Hybrid Nanomaterials Built from Metal—Ligand Coordination Bonds: Nanoscale Metal—Organic Frameworks and Nanoscale Coordination Polymers. Chem. Rev. 2015, 115, 11079—11108.
- (21) Wang, L.; Zheng, M.; Xie, Z. Nanoscale Metal—Organic Frameworks for Drug Delivery: a Conventional Platform with New Promise. J. Mater. Chem. B 2018, 6, 707—717.
- (22) Stavila, V.; Talin, A. A.; Allendorf, M. D. MOF-Based Electronic and Optoelectronic Devices. *Chem. Soc. Rev.* **2014**, *43*, 5994–6010.
- (23) So, M. C.; Wiederrecht, G. P.; Mondloch, J. E.; Hupp, J. T.; Farha, O. K. Metal-Organic Framework Materials for Light-Harvesting and Energy Transfer. *Chem. Commun.* **2015**, *51*, 3501–3510.
- (24) Stassen, I.; Burtch, N.; Talin, A.; Falcaro, P.; Allendorf, M.; Ameloot, R. An Updated Roadmap for the Integration of Metal—Organic Frameworks with Electronic Devices and Chemical Sensors. *Chem. Soc. Rev.* **2017**, *46*, 3185–3241.
- (25) Batten, S. R.; Robson, R. Interpenetrating Nets: Ordered, Periodic Entanglement. *Angew. Chem., Int. Ed.* **1998**, *37*, 1460–1494.
- (26) Kitagawa, S.; Kondo, M. Functional Micropore Chemistry of Crystalline Metal Complex-Assembled Compounds. *Bull. Chem. Soc. Jpn.* 1998, 71, 1739–1753.
- (27) Yaghi, O. M.; O'Keeffe, M.; Kanatzidis, M. Design of Solids from Molecular Building Blocks: Golden Opportunities for Solid State Chemistry. *J. Solid State Chem.* **2000**, *152*, 1–2.
- (28) Férey, G. Building Units Design and Scale Chemistry. J. Solid State Chem. 2000, 152, 37–48.
- (29) Yaghi, O. M.; O'Keeffe, M.; Ockwig, N. W.; Chae, H. K.; Eddaoudi, M.; Kim, J. Reticular Synthesis and the Design of New Materials. *Nature* **2003**, 423, 705.
- (30) Kalmutzki, M. J.; Hanikel, N.; Yaghi, O. M. Secondary Building Units as the Turning Point in the Development of the Reticular Chemistry of MOFs. *Sci. Adv.* **2018**, *4*, eaat9180.
- (31) Düren, T.; Bae, Y.-S.; Snurr, R. Q. Using Molecular Simulation to Characterise Metal—Organic Frameworks for Adsorption Applications. *Chem. Soc. Rev.* **2009**, *38*, 1237—1247.
- (32) Johnson, J. A.; Zhang, X.; Zhang, X.; Zhang, J. Recent Advances in Ionic Metal-Organic Frameworks: Design, Synthesis, and Application. *Curr. Org. Chem.* **2014**, *18*, 1973–2001.
- (33) Karmakar, A.; Desai, A. V.; Ghosh, S. K. Ionic Metal-Organic Frameworks (iMOFs): Design Principles and Applications. *Coord. Chem. Rev.* **2016**, *307*, 313–341.
- (34) Mavrandonakis, A.; Klontzas, E.; Tylianakis, E.; Froudakis, G. E. Enhancement of Hydrogen Adsorption in Metal-Organic Frameworks by the Incorporation of the Sulfonate Group and Li Cations. A Multiscale Computational Study. *J. Am. Chem. Soc.* **2009**, *131*, 13410–13414.
- (35) Higuchi, M.; Nakamura, K.; Horike, S.; Hijikata, Y.; Yanai, N.; Fukushima, T.; Kim, J.; Kato, K.; Takata, M.; Watanabe, D.; Oshima, S.; Kitagawa, S. Design of Flexible Lewis Acidic Sites in Porous

- Coordination Polymers by Using the Viologen Moiety. *Angew. Chem., Int. Ed.* **2012**, *51*, 8369–8372.
- (36) Pan, M.; Du, B.-B.; Zhu, Y.-X.; Yue, M.-Q.; Wei, Z.-W.; Su, C.-Y. Highly Efficient Visible-to-NIR Luminescence of Lanthanide(III) Complexes with Zwitterionic Ligands Bearing Charge-Transfer Character: Beyond Triplet Sensitization. *Chem. Eur. J.* **2016**, 22, 2440–2451.
- (37) Aulakh, D.; Varghese, J. R.; Wriedt, M. A New Design Strategy to Access Zwitterionic Metal—Organic Frameworks from Anionic Viologen Derivates. *Inorg. Chem.* **2015**, *54*, 1756—1764.
- (38) Aulakh, D.; Nicoletta, A. P.; Varghese, J. R.; Wriedt, M. The Structural Diversity and Properties of Nine New Viologen Based Zwitterionic Metal—Organic Frameworks. *CrystEngComm* **2016**, *18*, 2189—2202.
- (39) An, W.; Aulakh, D.; Zhang, X.; Verdegaal, W. M.; Dunbar, K. R.; Wriedt, M. Switching of Adsorption Properties in a Zwitterionic Metal-Organic Framework Triggered by Photogenerated Radical Triplets. *Chem. Mater.* **2016**, *28*, 7825–7832.
- (40) Aulakh, D.; Nicoletta, A. P.; Pyser, J. B.; Varghese, J. R.; Wriedt, M. Design, Structural Diversity and Properties of Novel Zwitterionic Metal—Organic Frameworks. *Dalton Trans.* **2017**, *46*, 6853—6869.
- (41) Aulakh, D.; Islamoglu, T.; Bagundes, V. F.; Varghese, J. R.; Duell, K.; Joy, M.; Teat, S. J.; Farha, O. K.; Wriedt, M. Rational Design of Pore Size and Functionality in a Series of Isoreticular Zwitterionic Metal-Organic Frameworks. *Chem. Mater.* **2018**, *30*, 8332–8342.
- (42) Zhang, J.; Zhao, M.; Xie, W.; Jin, J.; Xie, F.; Song, X.; Zhang, S.; Wu, J.; Tian, Y. A Series of Novel Cadmium(II) Coordination Polymers with Photoluminescence and Ferroelectric Properties Based on Zwitterionic Ligands. *New J. Chem.* **2017**, *41*, 9152–9158.
- (43) Grigolo, T. A.; de Campos, S. D.; Manarin, F.; Botteselle, G. V.; Brandão, P.; Amaral, A. A.; de Campos, E. A. Catalytic Properties of a Cobalt Metal—Organic Framework with a Zwitterionic Ligand Synthesized In Situ. *Dalton Trans.* **2017**, *46*, 15698—15703.
- (44) Qin, L.; Sun, Z.-Y.; Cheng, K.; Liu, S.-W.; Pang, J.-X.; Xia, L.-M.; Chen, W.-H.; Cheng, Z.; Chen, J.-X. Zwitterionic Manganese and Gadolinium Metal—Organic Frameworks as Efficient Contrast Agents for in Vivo Magnetic Resonance Imaging. ACS Appl. Mater. Interfaces 2017, 9, 41378—41386.
- (45) Zhang, C.; Liu, Y.; Sun, L.; Shi, H.; Shi, C.; Liang, Z.; Li, J. A Zwitterionic Ligand-Based Cationic Metal-Organic Framework for Rapidly Selective Dye Capture and Highly Efficient $\text{Cr}_2\text{O}_7^{2-}$ Removal. *Chem. Eur. J.* **2018**, 24, 2718–2724.
- (46) Wang, S.; Yang, Q.; Zhang, J.; Zhang, X.; Zhao, C.; Jiang, L.; Su, C.-Y. Two-Dimensional Charge-Separated Metal—Organic Framework for Hysteretic and Modulated Sorption. *Inorg. Chem.* **2013**, *52*, 4198—4204.
- (47) Lalonde, M. B.; Getman, R. B.; Lee, J. Y.; Roberts, J. M.; Sarjeant, A. A.; Scheidt, K. A.; Georgiev, P. A.; Embs, J. P.; Eckert, J.; Farha, O. K.; Snurr, R. Q.; Hupp, J. T. A Zwitterionic Metal—Organic Famework with Free Carboxylic Acid Sites that Exhibits Enhanced Hydrogen Adsorption Energies. *CrystEngComm* **2013**, *15*, 9408—9414.
- (48) Johnson, J. A.; Petersen, B. M.; Kormos, A.; Echeverria, E.; Chen, Y.-S.; Zhang, J. A New Approach to Non-Coordinating Anions: Lewis Acid Enhancement of Porphyrin Metal Centers in a Zwitterionic Metal—Organic Framework. J. Am. Chem. Soc. 2016, 138, 10293—10298.
- (49) Guo, Y.; Jiang, Z.; Wang, X.; Ying, W.; Chen, D.; Liu, S.; Chen, S.; Jiang, Z.-J.; Peng, X. Zwitterion Threaded Metal—Organic Framework Membranes for Direct Methanol Fuel Cells. *J. Mater. Chem. A* **2018**, *6*, 19547—19554.
- (50) Hamilton, B. H.; Cardon, T. B.; Lorigan, G. A.; Ziegler, C. J. The assembly of organic radical anions between metal-borate scaffolds. *Dalton Trans.* **2005**, 2941–2944.
- (51) Hamilton, B. H.; Kelly, K. A.; Wagler, T. A.; Espe, M. P.; Ziegler, C. J. Construction of a Functional Layered Solid Using the Tetrakis(imidazolyl)borate Coordinating Anion. *Inorg. Chem.* **2002**, *41*, 4984–4986.

- (52) Hamilton, B. H.; Ziegler, C. J. Lead and Thallium Tetrakis-(imidazolyl)borates: Modifying Structure by Varying Metal and Anion. *Inorg. Chem.* **2004**, 43, 4272–4277.
- (53) Hamilton, B. H.; Wagler, T. A.; Espe, M. P.; Ziegler, C. J. Sequestering Perrhenate with a Borate-Based Coordination Polymer: A Model for Pertechnetate Separation. *Inorg. Chem.* **2005**, *44*, 4891–4893.
- (54) Hamilton, B. H.; Kelly, K. A.; Wagler, T. A.; Espe, M. P.; Ziegler, C. J. Lead Tetrakis(imidazolyl)borate Solids: Anion Exchange, Solvent Intercalation, and Self Assembly of an Organic Anion. *Inorg. Chem.* **2004**, *43*, 50–56.
- (55) Hamilton, B. H.; Kelly, K. A.; Malasi, W.; Ziegler, C. J. Tetrakis(imidazolyl)borate-Based Coordination Polymers: Group II Network Solids, M[B(Im)4]2(H2O)2 (M) Mg, Ca, Sr). *Inorg. Chem.* **2003**, 42, 3067–3073.
- (56) Thapa, S.; Hettiarachchi, E.; Dickie, D. A.; Rubasinghege, G.; Qin, Y. A Charge-Separated Diamondoid Metal—Organic Framework. *Chem. Commun.* **2018**, *54*, 12654—12657.
- (57) Türp, D.; Wagner, M.; Enkelmann, V.; Müllen, K. Synthesis of Nanometer-Sized, Rigid, and Hydrophobic Anions. *Angew. Chem., Int. Ed.* **2011**, *50*, 4962–4965.
- (58) Fischer, S.; Schmidt, J.; Strauch, P.; Thomas, A. An Anionic Microporous Polymer Network Prepared by the Polymerization of Weakly Coordinating Anions. *Angew. Chem., Int. Ed.* **2013**, *52*, 12174–12178.
- (59) Burgun, A.; Crees, R. S.; Cole, M. L.; Doonan, C. J.; Sumby, C. J. A 3-D Diamondoid MOF Catalyst Based on In Situ Generated [Cu(L)2] N-Heterocyclic Carbene (NHC) Linkers: Hydroboration of CO₂. Chem. Commun. **2014**, 50, 11760–11763.
- (60) Xiao, Y.-J.; Sun, C.-Y.; Yang, G.-C.; Zhao, L.; Su, Z.-M. A Versatile Metal-Organic Framework for Carbon Dioxide Capture and Modulating Fluorescence Properties of Alq3. *Inorg. Chem. Commun.* **2014**, *46*, 248–250.
- (61) MacGillivray, L. R.; Subramanian, S.; Zaworotko, M. J. Interwoven Two- and Three-Dimensional Coordination Polymers through Self-Assembly of CuI Cations with Linear Bidentate Ligands. *J. Chem. Soc., Chem. Commun.* 1994, 1325–1326.
- (62) Blake, A. J.; Champness, N. R.; Chung, S. S. M.; Li, W.-S.; Schröder, M. Control of Interpenetrating Copper(i) Adamantoid Networks: Synthesis and Structure of {[Cu(bpe)2]BF4}n. *Chem. Commun.* 1997, 1005–1006.
- (63) Ryan, P. E.; Lescop, C.; Laliberté, D.; Hamilton, T.; Maris, T.; Wuest, J. D. Engineering New Metal-Organic Frameworks Built from Flexible Tetrapyridines Coordinated to Cu(II) and Cu(I). *Inorg. Chem.* **2009**, *48*, 2793–2807.
- (64) Ray, S.; Zalkin, A.; Templeton, D. H. Crystal Structure of Copper Fluosilicate Hexahydrate. *Acta Crystallogr., Sect. B: Struct. Crystallogr. Cryst. Chem.* **1973**, 29, 2748–2751.
- (65) Zibaseresht, R.; Hartshorn, R. M. Hexaaquacopper(II) Dinitrate: Absence of Jahn-Teller Distortion. *Acta Crystallogr., Sect. E: Struct. Rep. Online* **2006**, 62, i19–i22.